

This manuscript has been authored by UT-Battelle, LLC under Contract No. DE-AC05-00OR22725 with the U.S. Department of Energy. The United States Government retains and the publisher, by accepting the article for publication, acknowledges that the United States Government retains a non-exclusive, paid-up, irrevocable, world-wide license to publish or reproduce the published form of this manuscript, or allow others to do so, for United States Government purposes. The Department of Energy will provide public access to these results of federally sponsored research in accordance with the DOE Public Access Plan(<http://energy.gov/downloads/doe-public-access-plan>)

Heat-Treated Aerogel as a Catalyst for Oxygen Reduction Reaction

Noam Zion,¹ David A. Cullen,² Piotr Zelenay,^{3*} Lior Elbaz^{1*}

¹ Bar-Ilan University, Ramat-Gan 52900, Israel

² Oak Ridge National Laboratory, Oak Ridge, TN 37831, USA

³ Los Alamos National Laboratory, Los Alamos, NM 87545, USA

*Corresponding authors E-mails: zelenay@lanl.gov; lior.elbaz@biu.ac.il

Abstract

Aerogels are fascinating materials that could be used for a wide range of applications, one of which is electrocatalysis of the important oxygen reduction reaction. In their inorganic form, aerogels can have ultra-high catalytic site density, high surface area, and tunable physical properties and chemical structures - important features in heterogeneous catalysis. Herein, we report on the synthesis and electrocatalytic properties of an iron-porphyrin aerogel. 5,10,15,20-(tetra-4-aminophenyl)porphyrin (H₂TAPP) and Fe(II) were used as building blocks of the aerogel, which was later heat-treated at 600 °C to enhance electronic conductivity and catalytic activity, while preserving its macro-structure. The resulting material has a very high concentration of atomically dispersed catalytic sites (9.7 10²⁰ sites g⁻¹), capable of catalyzing the oxygen reduction reaction in alkaline solution ($E_{onset} = 0.92$ V vs. RHE, TOF = 0.25 e⁻ site⁻¹ s⁻¹ at 0.80 V vs. RHE).

Introduction

The oxygen-reduction reaction (ORR) is one of the most important reactions in nature. Its relatively slow kinetics is catalyzed by various enzymes to facilitate a wide range of processes in biological systems, from metabolism to respiration. In nature, transition metal complexes, mainly metallo-porphyrins, are the catalytic centers in enzymes such as cytochrome C oxidase. The interest in the catalysis of this reaction increased in recent years due to its critical role in some alternative energy technologies, requiring high reaction rate and thermodynamic efficiency. Although platinum-group metals (PGM) can catalyze the ORR quite effectively, their major drawbacks are limited availability and high cost.^[1] Other issues, which may be even more important, are limited long-term durability and low chemical stability of catalyst supports, usually carbon-based.^[2]

In the past couple of decades, great advancements have been made in the development of PGM-free catalysts based on earth-abundant elements, nitrogen, carbon and transition metals (usually Fe or Co), inspired by biological systems such as porphyrins and phthalocyanines.^[1a, 3] In order to overcome the poor stability and low catalytic activity of transition-metal complexes, a class of high temperature-treated (HT-treated) catalysts, composed of the same elements, *i.e.*, a transition metal, carbon and nitrogen, was developed. Although HT-treated PGM-free catalysts exhibit improved activity and stability, their performance remains inferior to PGM catalysts, calling for further improvements to make PGM-free catalysts a viable alternative to the state-of-the-art materials. The improvements need to address the intrinsically low

turnover frequency, which can be compensated by forming some highly dense catalytic frameworks.^[4]

In this work, we designed, synthesized and characterized ORR catalysts based on iron, carbon and nitrogen in a well-defined, high surface-area covalent organic framework (COF) aerogels. Aerogels are ultralight, porous materials with ultra-low density and high void volume (>97%). They are known for their unique physicochemical properties such as high porosity, controllable pore size and surface area, and low thermal conductivity, just to name a few.^[5] The variety of precursors used for the synthesis of aerogels makes them promising candidates for a wide range of applications in catalysts, capacitors, insulators, absorbents, etc.^[6]

Results and discussion

Metallo-porphyrin aerogels were synthesized here through a metalation-gelation process, as described in the experimental section and in **Scheme 1**. This method was developed to prevent aggregation of the porphyrin prior to the reaction.^[7] A three-dimensional COF-porphyrin aerogel and 30 mg of porphyrin powder used for its synthesis are shown on the right and left sides in **Fig. 1**, respectively.

The porphyrin molecules in the aerogel are connected through their amine substituent, as divulged by an FTIR-ATR spectrum of the gel in **Fig. 2**. The peak at 1621 cm^{-1} is attributed to a newly formed C=N bond linking between porphyrin monomers, expected for the imine groups. This is supported by NMR spectra recorded during the reaction, which reveal a new peak at 161 ppm, attributed to the same

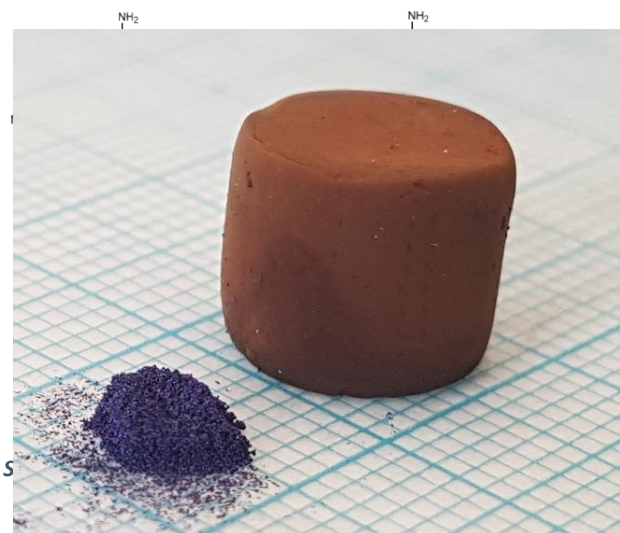


Figure 1: Image of 30 mg of porphyrin powder (left) and the porphyrin aerogel synthesized from the same amount of porphyrin (right).

bridging bond (**Fig. S1**). Since it is well-established that transition metal complexes in general, and metalloporphyrins in particular, can efficiently catalyze ORR through their metal center, Fe was incorporated into the porphyrin aerogel during the gel formation, as described in the experimental section. It is important to note that the timing of metal insertion was critical for the formation of the aerogel. When Fe(III)TAPP (FeP) was used as the precursor, aggregates were formed in the solution as a result of the coordination of aminophenyl groups in neighboring porphyrins to the metal ion.^[8] To avoid aggregate formation, the metal ion was added during the polymerization of the free-base porphyrin.

Several techniques were used to study coordination of the Fe ion by the porphyrin after the aerogel formation. In free-base porphyrins, two out of four pyrroles have hydrogen bonded to nitrogen, and the stretch of the N-H bond can be seen at 3322 cm^{-1} in the FTIR-ATR spectra (**Fig. S2**). After the metalation, this peak disappears, indicating successful deprotonation of the pyrrole ligands in the porphyrin core, a necessary step for the metalation reaction.^[9]

The interaction between the metal ion and the pyrrolic nitrogen atoms in the porphyrin aerogel was investigated by XPS. The N 1s spectrum can be de-convoluted into five distinct peaks, with the most pronounced of them occurring at a binding energy of 398.79 eV (**Fig. 3**). This N 1s peak is assigned to the new N-Fe bond formed with the porphyrin center during the aerogel synthesis, which is not present in similar porphyrins devoid of the Fe.^[10] The peak located at 400.08 eV is related to pyrrolic groups.^[11]

Charged nitrogen species, originated from amine or imine like bonds, can be shown at 401.78 eV.^[12] The Fe 2p spectrum reveals trivalent iron with peaks at binding energies of 711.31 and 724.83 eV, supporting coordination of iron ion to pyrrolic nitrogen in the porphyrin core.^[13] The calculated N:Fe atomic ratio is 8.57:1, very close to the theoretical ratio expected for FeP (8:1), which points to a high metalation yield (*ca.* 93%). It is important to note that

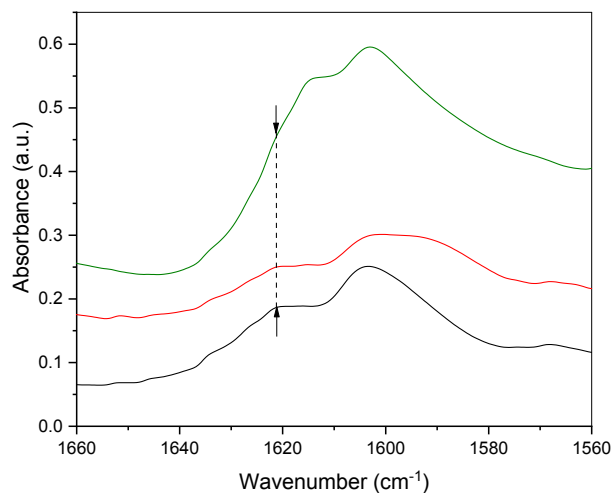
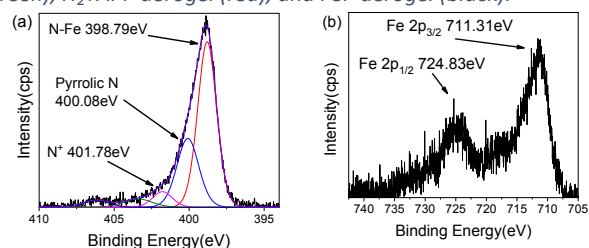


Figure 2: FTIR-ATR comparison of H₂TAPP monomer powder (green), H₂TAPP aerogel (red), and FeP aerogel (black).



no metallic iron or iron oxide were found in the aerogel.

Figure 3: XPS spectra of a) N 1s b) Fe 2P in the FeP aerogel.

In its organic form, the FeP aerogel was found to have a relatively low electronic conductivity. Since the prerequisite of any electrode material is high electronic conductivity, the FeP aerogel was heat-treated under inert atmosphere. From the vast knowledge accumulated in this field over several decades of research efforts, the optimum temperature range for the pyrolysis of macrocyclic compounds is between 600 to 1000 °C.^[14] In this range, the compounds are partially decomposed, mainly to NO_x and CO_x, and graphitic carbonaceous material is formed. The heat-treatment conditions for porphyrin aerogels were studied here and optimized using TGA-MS. During the treatment of the H₂TAPP aerogel two main weight-loss steps were observed at 350 °C (15%) and 670 °C (32%) (**Fig. S3**), whereas four main steps were observed for the FeP aerogel at 500 °C (21.4%), 630 (21.3%), 710 (8.4%) and 850 °C (10.5%). In both cases, the most significant mass loss took place between 500 and 710 °C. Mass spectroscopy shows that the weight loss of both iron and free-base porphyrin aerogels is due to a loss of carbonaceous compounds and small amounts of acetone remaining in the pores after the synthesis (in spite of several rinses with liquid CO₂ during the supercritical drying procedure; described in the experimental section).

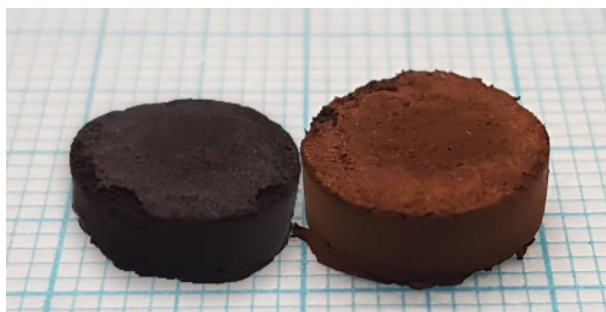


Figure 4: Picture of FeP aerogel after heat-treatment (left) and FeP aerogel before heat-treatment (right).

The integrity of the catalytic center depends on maintaining transition-metal coordination by nitrogen atoms, which tends to be lost at temperatures above 600 °C. In order to preserve the activity and site density of these presumed catalytic sites, the heat-treatment temperature was limited to 600 °C. The immediate physical result of this low-temperature heat-treatment (LTHT) was a change in the aerogel color, from brown to black, accompanied by a relatively small volume change and no apparent change in the aerogel macro structure (**Fig. 4**).

As expected, the electronic conductivity of the aerogel increased significantly, from virtually none to 2.7 S cm⁻¹, *i.e.*, very close to that of commercial Vulcan XC72 (4.3 S cm⁻¹) and about twice that of carbon RF aerogel (1.32 S cm⁻¹).^[15]

The morphology of the FeP aerogel subjected to LTHT (LTHT-FeP) was studied using HR-SEM (**Fig. 5**). The aerogel maintained its porosity and physical structure after the LTHT. The BET surface area of the LTHT-FeP aerogel was 191 m²/g (312 m²/g before LTHT treatment).

XPS characterization of the LTHT-FeP aerogel reveals the presence of the N-Fe bond at 398.3 eV,^[16] also observed with the non-heat-treated aerogel. No metallic Fe was detected in the LTHT-FeP aerogel, with all iron remaining in the Fe(III) state. From XPS, the N-to-Fe atomic ratio was found to be 6.5:1, which is less than that of *ca.* 8:1 before the heat treatment (**Fig. 6a**). The small shift in the N-Fe bond energies observed after the LTHT can be attributed to the loss of the Cl⁻ counter ion, which was coordinated to the Fe in the porphyrin in the FeP aerogel. The Fe-to-Cl atomic ratio increased from 1.48:1 before the LTHT, to 5.27:1 after LTHT, indicating that fewer chloride counter ions are involved in the coordination bond with the iron after the heat treatment. Change of ligands during LTHT leads to changes in binding energies of Fe, as indicated by both Fe 2p and N 1s spectra before and after LTHT.^[17] The most significant N 1s peak is assigned to pyrrolic-N at 399.9 eV, indicating that the iron-ion environment does not change significantly after the LTHT. Graphitic-N was also detected in the LTHT-FeP, which could originate from either non-reacted aniline groups in the porphyrin or the cross-linked imine bond. These results are in full agreement with Fe 2p 3/2 spectra (**Fig. 6b**).

From mass balance, verified by induced coupled plasma (ICP) measurements, the iron content in the aerogels synthesized here is 6.4 wt.% and 9.0 wt.% for the FeP aerogel and LTHT-FeP aerogel, respectively. To the best of the authors' knowledge, this is the highest content of atomically dispersed Fe(III) in a PGM-free ORR

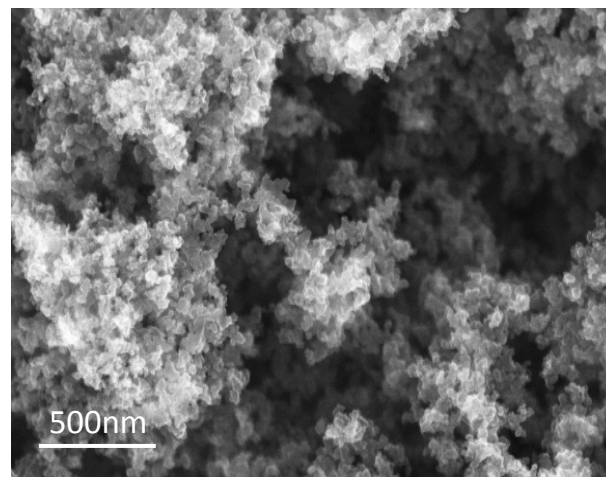
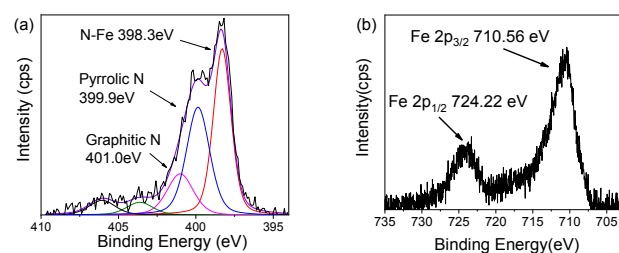


Figure 5: HR-SEM of LTHT-FeP aerogel.



catalyst. To put the importance of this number into perspective, the relatively low oxygen turnover frequency (TOF) and low Fe content in PGM-free catalysts require high catalyst loading in the

Figure 6: (a) N 1s and (b) Fe 2P XPS spectra of LTHT-FeP aerogel.

fuel cell cathodes, significantly increasing their thickness. Such electrodes tend to suffer from poor mass transfer of reactants and products to and from catalytic centers. The benchmark today is below 2 wt.% of atomically dispersed iron ions.^[18]

A high surface-area, very porous aerogel with density of only 42 and 39 mg/cm³, before and after the LTHT, respectively, consisting only of metal ions and coordinating ligands (presumed catalytic centers), yields material with the highest volumetric density of catalytic sites. Consequently, aerogels have the potential of becoming important materials for heterogeneous catalysis in general and electrocatalysis of ORR in particular. Assuming all the Fe(III) sites are available for electrocatalysis, the calculated density of catalytic sites in the aerogel is 3.3 10¹⁹ sites cm⁻³ before the heat treatment and 4.0 10¹⁹ sites cm⁻³ after the LTHT (based on mass and volume measurements). The observed *ca.* 9.5% increase in the presumed active-site density after the heat treatment is attributed to a “shrinkage” of the aerogel following the heat treatment. The site density in the LTHT-FeP aerogel is one order of magnitude higher than in the state-of-the-art PGM-free catalysts today,^[18-19] and very close to the target active site density of 3.1 10²⁰ sites cm⁻³, suggested by Gasteiger *et al.* for PGM-free polymer electrolyte fuel cell (PEFC) cathode catalysts.^[4c]

Annular dark-field STEM (HAADF-STEM) images and electron energy loss point spectra (EELS) (**Fig. 7**)

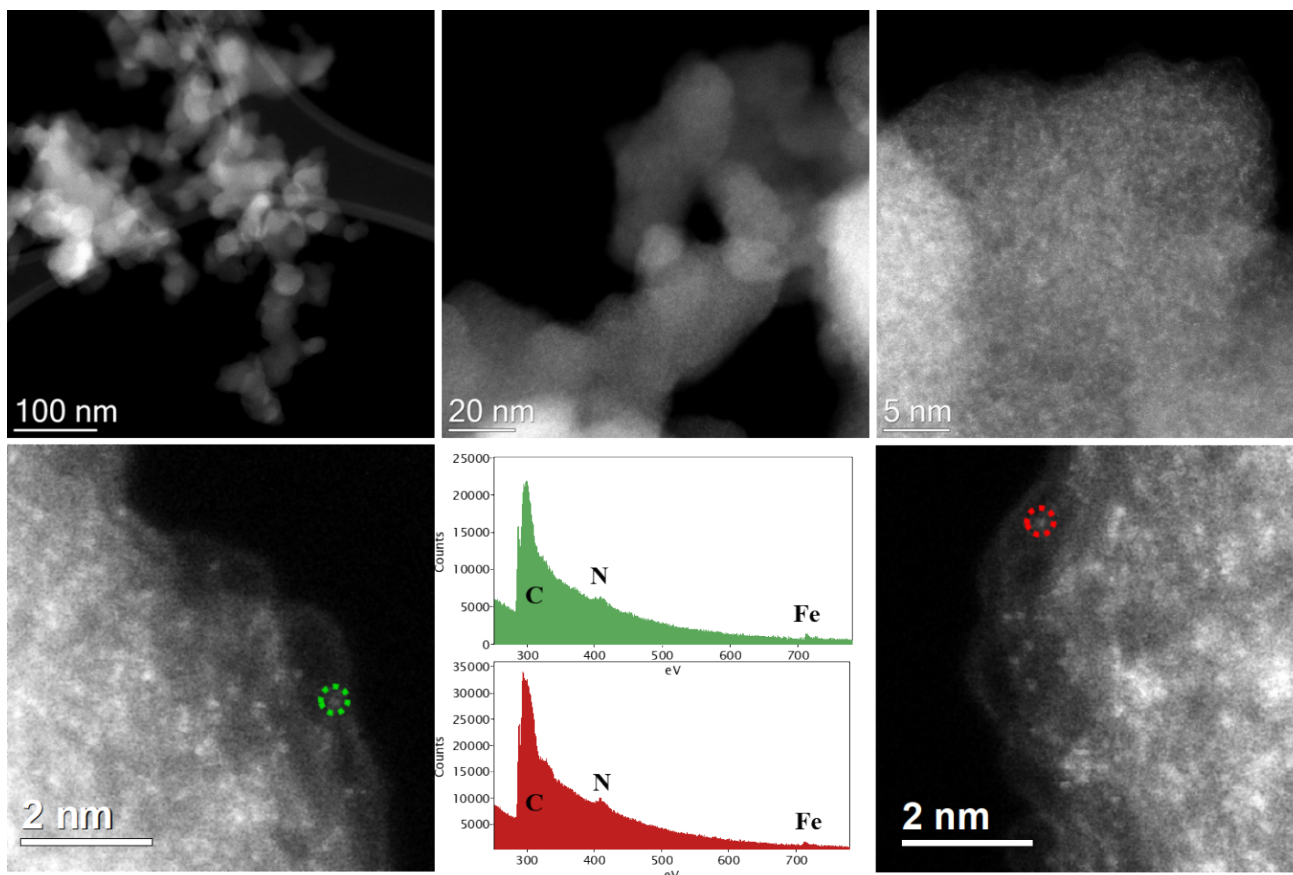
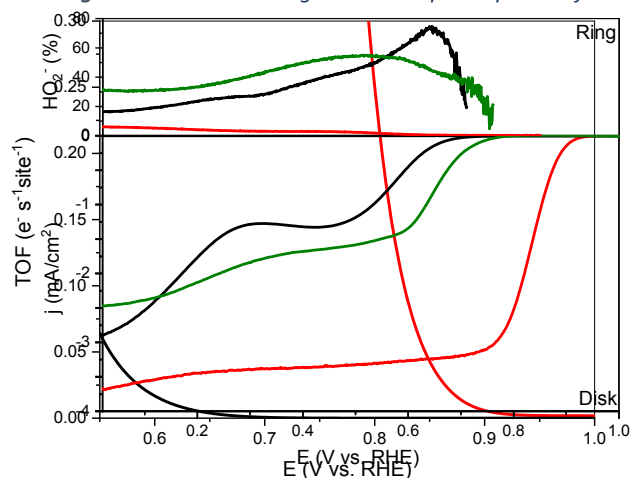


Figure 7: ADF-STEM images and EELS point spectra of LTHT-FeP aerogel (red and green circles are the positions of the recorded EELS)



show that the nanoparticles observed in the HR-SEM image are composed of atomically dispersed Fe atoms imbedded in nitrogen-doped carbonaceous material. Despite the high Fe loading, no Fe nanoparticles were found in the sample, although some clustering was observed. Aerogels are not 2D materials, which makes precise determination of the surface concentration of metal ions difficult using this method. However, the very number of atoms in the image depicting a very small volume of the catalyst (cross-section of a few nm²), indicates a high transition-metal concentration and, correspondingly, a high number of the catalytic sites to compensate for the low ORR turnover frequency.^[20] Quantification of EELS data obtained from several particles showed the N-to-Fe atomic ratio to be 6.9:1.0 and 8.3:1.0 for the LTHT FeP and FeP

Figure 9: Calculated turnover frequencies of LTHT-FeP aerogel (red) and FeP aerogel (black).

ul 500 ipm.

aerogels, respectively, in excellent agreement to XPS results. The EEL point spectra confirm the observed atoms are Fe, and the presence of N within the spectra corroborates the Fe-N bonding observed by XPS.

The ORR catalytic activity of the newly synthesized aerogels was studied using rotating ring disk electrode (RRDE) in alkaline environment (**Fig. 8**). The LTHT-FeP aerogel was compared to the FeP aerogel and LTHT-P aerogel. The LTHT-FeP aerogel shows significantly higher performance with $E_{onset} = 0.92$ V and $E_{1/2} = 0.83$ V vs. RHE, whereas the E_{onset} measured with the LTHT-P aerogel, devoid of any metal, is only 0.76 V and $E_{1/2} = 0.65$ V vs. RHE, still higher than the $E_{onset} = 0.69$ V and $E_{1/2} = 0.57$ V

vs. RHE, obtained with FeP aerogel. The limiting current density measured with the LTHT-FeP aerogel attests to four-electron oxygen reduction to water, whereas the limiting current values measured with LTHT-P aerogel and FeP aerogel point to the undesirable two-electron reduction of oxygen to hydrogen peroxide. This is also supported by the ring currents, showing the amount of HO₂⁻ produced during the reaction as function of the disk potential. At the LTHT-FeP aerogel, the peroxide anion yield changes from zero at high potentials (0.92–0.72 V vs. RHE) to 6% at 0.02 V vs. RHE. It is much lower than peroxide yield values measured with both FeP and LTHT-P aerogels, 14 and 31% at 0.02 V vs. RHE, respectively.

The turnover frequency (TOF) values in **Fig. 9**, were calculated from the RDE kinetic current data and site density values, assuming that all sites are available for ORR electrocatalysis.^[21] They were found to be 0.065 e⁻ site⁻¹ s⁻¹ at 0.55 V vs. RHE and 0.25 e⁻ site⁻¹ s⁻¹ at 0.8 V vs. RHE for the FeP and LTHT-FeP aerogels, respectively.^[20a] The TOF values obtained with the LTHT-FeP correspond to approximately half of those measured with Pt-based catalysts. In their study of the state-of-the-art PGM-free catalysts, Strasser *et al.* reported a TOF value of 0.7 e⁻ site⁻¹ s⁻¹ for Fe-N-C catalyst in 0.1 M KOH at 0.8 V vs. RHE, after two heat-treatments and acid leaching.^[22] While the TOF values differ by a factor of approximately three in favor of the Fe-N-C catalyst, the LTHT-FeP promises to have more potential as a catalyst/support system when compared to other PGM-free catalysts owing to the very high number of active sites, 9.7 10²⁰ sites g⁻¹ (calculated from ICP measurements), an order of magnitude higher than that measured with Fe-N-C by Strasser *et al.* using CO adsorption.^[22]

Conclusions

In this work, we succeeded at synthesizing a structurally stable iron porphyrin aerogel exhibiting high surface area and very high density of the likely ORR catalytic sites. The aerogel was heat-treated at a relatively low temperature in order to increase its electronic conductivity while minimizing the effect on the aerogel macrostructure and Fe coordination. Atomically dispersed iron ions were found to be uniformly distributed in three-dimensional aerogels before and after the heat treatment. In spite of shrinking by *ca.* 9.5% following the heat treatment, the LTHT-FeP aerogel structure remained intact. The resulting aerogel ORR catalyst was found to have a record high density of atomically dispersed iron sites.

Experimental

Aerogels synthesis

The aerogels in this work were synthesized from tetra-4-aminophenyl porphyrin, which served as a gel monomer, *via* a polycondensation reaction of the amine substituents on the porphyrin ring with aldehyde cross-linkers, following known recipes involving amine-substituted monomers.^[23] The porphyrin aerogels were synthesized according to the following procedure: 15 mg of iron(II) chloride tetrahydrate (FeCl₂·4H₂O 99+%, ARCOS

ORGANICS), was dissolved in 250 μl dimethyl sulfoxide (DMSO), followed by the addition of the monomer for the polymerization, 10 mg of a free base porphyrin, 5,10,15,20-(tetra-4-aminophenyl)porphyrin (TAPP) (98%, PorphyChem). The solution was heated to 80 °C and stirred for 30 minutes, for the metal insertion process. To form the gel, a solution containing the terephthalaldehyde (98%, Alfa Aesar) cross-linker was dissolved in DMSO with a 1:2 molar ratio of –NH₂ to –CHO. 250 μL of the cross-linker solution was added dropwise to the porphyrin solution. The new solution was heated to 80 °C and stirred for 10 seconds (the magnetic stirrer was immediately pulled out due to the fast gelation). (Scheme 1). Once formed, the gel was washed with fresh DMSO once a day, for four consecutive days, to remove unreacted chemicals until no residues were seen in the solvent above the gel. Then, the gel was washed with acetone in order to replace the DMSO in the pores. Finally, the gel was dried using CO₂ under supercritical conditions in a critical-point dryer (tousimis® 931GL) to yield the aerogel.

The heat treatment was carried out in a glass-tube oven (Thermo Scientific-Lindberg Blue M) under argon (MAXIMA). The temperature was increased from 25 °C to 600 °C for five hours (*i.e.*, at a rate of 2 °C/min) and then held at 600 °C for two hours.

Methods

The porphyrin aerogels were characterized using a Nicolet iS50 Fourier transform infrared spectroscopy-attenuated total reflectance (FTIR-ATR) instrument (Thermo Scientific). An Ocean Optics DH-2000-BAL ultraviolet-visible spectrophotometer (UV-Vis) was used to verify the metalation of the aerogel. X-ray photoelectron spectroscopy (XPS) measurements were performed with Kratos AXIS ULTRA system using a monochromatic Al K_α X-ray source (hν = 1486.6 eV) at 75 W and detection pass energies ranging between 20 and 80 eV. Curve-fitting analysis was based on linear or Shirley background subtraction and application of Gaussian-Lorentzian line shapes.

Conductivity measurements^[24] were performed using electronic micrometer (INSIZE) and referenced to those of Vulcan XC72 (Cabot), LTHT-P aerogel and heat-treated resorcinol-formaldehyde (RF) aerogel synthesized according to a method described by Pekala *et al.*^[25] The thermal gravimetric analysis (TGA-GC-MS (EI/CI) was carried out using Clarus 680/Clarus SQ 8C, by Perkin Elmer.

The morphology of the aerogel was studied using high-resolution scanning electron microscope (HRSEM) Magellan 400L. To examine the size, shape, and content of the particles, high-resolution scanning transmission electron microscope (Nion UltraSTEM U100 operated at 60kV) was used. The surface area of the heat-treated aerogel was measured and calculated from the Brunauer–Emmett–Teller (BET) N₂ adsorption isotherm at 77 K (Quantachrome Autosorb iQ).

Nuclear magnetic resonance (NMR) measurement of the porphyrin was performed in DMSO using Bruker 700 Hz spectrometer. To verify the crosslinking site,

terephthalaldehyde solution (in DMSO) was added in portions over time.

Induced coupled plasma (SPECTRO ARCOS ICP OES, FHX22, MultiView plasma) was performed for FeP. The sample was prepared by heating under air, at 800 °C, overnight, 2.82 mg of FeP. The iron remained after the treatment, was dissolved in concentrated 1:1 HCl:HNO₃, and diluted for the analysis.

Electrochemistry

The electrochemical measurements were conducted in 0.1 M KOH (Acros, 99.98%) using Bio-Logic VMP 300 bipotentiostat) 10 mg of the HT-FeP aerogel was grinded and suspended in 1 mL of 2/3 isopropanol: 1/3 de-ionized water (volume ratio). Then, 10 µL of the aerogel slurry was deposited onto a glassy-carbon rotating ring disk electrode (Pine, 5.61 mm diameter). The reference electrode was a reversible hydrogen electrode (RHE, platinized platinum in the electrolyte solution bubbled with pure hydrogen, 99.99%) and the counter electrode that was used is a glassy carbon rod.

The ORR with all materials synthesized in this work was studied by rotating ring disk electrode (RRDE). The ORR polarization plots were conducted using 5 mV/s scan rate at 900 rpm, between 0.02 V and 1.0 V vs. RHE. All measurements were background current-corrected. The onset potentials were defined as the potential at 20 µA/cm².

Acknowledgments

This work was conducted in the framework of the Israeli Fuel Cells Consortium (part of the Israeli National Center for Electrochemical Propulsion), and partially funded by the Israeli Ministry of Energy, the Israeli Science Foundation, and United States-Israel Binational Science Foundation. High resolution STEM imaging was conducted at the Center for Nanophase Materials Sciences, which is a DOE Office of Science User Facility. This research was partially supported by a grant from the DOE-EERE Fuel Cell Technologies Office.

References

- [1] aZ. Chen, D. Higgins, A. Yu, L. Zhang, J. Zhang, *Energy & Environmental Science* **2011**, *4*, 3167-3192; bF. Jaouen, E. Proietti, M. Lefèvre, R. Chenitz, J.-P. Dodelet, G. Wu, H. T. Chung, C. M. Johnston, P. Zelenay, *Energy & Environmental Science* **2011**, *4*, 114-130.
- [2] aR. Borup, J. Meyers, B. Pivovar, Y. S. Kim, R. Mukundan, N. Garland, D. Myers, M. Wilson, F. Garzon, D. Wood, *Chemical reviews* **2007**, *107*, 3904-3951; bJ. C. Meier, C. Galeano, I. Katsounaros, A. A. Topalov, A. Kostka, F. Schüth, K. J. Mayrhofer, *Acs Catalysis* **2012**, *2*, 832-843.
- [3] aN. Zion, A. Friedman, N. Levy, L. Elbaz, *Advanced Materials* **2018**, 1800406; bR. Jasinski, *Nature* **1964**, *201*, 1212-1213; cN. Levy, A. Mohammed, A. Friedman, B. Gavriel, Z. Gross, L. Elbaz, *ChemCatChem* **2016**, *8*, 2832-2837; dN. Levy, A. Mohammed, M. Kosa, D. T. Major, Z. Gross, L. Elbaz, *Angew. Chem.-Int. Edit.* **2015**, *54*, 14080-14084; eR. Z. Snitkoff, N. Levy, I. Ozery, S. Ruthstein, L. Elbaz, *Carbon* **2019**, *143*, 223-229.
- [4] aH. A. Gasteiger, S. S. Kocha, B. Sompalli, F. T. Wagner, *Appl Catal B: Environ* **2005**, *56*, 9-35; bH. A. Gasteiger, N. M. Markovic, *Science* **2009**, *324*, 48-49; cF. T. Wagner, Gasteiger, H. A. and Yan, S. , in *Non-Platinum Electrocatalysts Workshop*, DOE, New Orleans, LA, **2003**.
- [5] L. W. Hrubesh, *Journal of Non-Crystalline Solids* **1998**, *225*, 335-342.
- [6] aS. Mayer, R. Pekala, J. Kaschmitter, *Journal of the Electrochemical Society* **1993**, *140*, 446-451; bM. A. Aegerter, N. Leventis, M. M. Koebel, *Aerogels handbook*, Springer Science & Business Media, **2011**; cJ. Marie, S. Berthon-Fabry, P. Achard, M. Chatenet, A. Pradourat, E. Chainet, *Journal of Non-Crystalline Solids* **2004**, *350*, 88-96; dC. Zhu, H. Li, S. Fu, D. Du, Y. Lin, *Chemical Society Reviews* **2016**, *45*, 517-531.
- [7] aK. S. Suslick, N. A. Rakow, M. E. Kosal, J.-H. Chou, *Journal of Porphyrins and Phthalocyanines* **2000**, *4*, 407-413; bJ. P. Collman, J. T. McDevitt, G. T. Yee, C. R. Leidner, L. G. McCullough, W. A. Little, J. B. Torrance, *Proceedings of the National Academy of Sciences of the United States of America* **1986**, *83*, 4581-4585.
- [8] M. Hanack, M. Lang, *Advanced Materials* **1994**, *6*, 819-833.
- [9] O. Herrmann, S. H. Mehdi, A. Corsini, *Canadian Journal of Chemistry* **1978**, *56*, 1084-1087.
- [10] aG. Wu, C. M. Johnston, N. H. Mack, K. Artyushkova, M. Ferrandon, M. Nelson, J. S. Lezama-Pacheco, S. D. Conradson, K. L. More, D. J. Myers, *Journal of Materials Chemistry* **2011**, *21*, 11392-11405; bU. Mazur, K. W. Hipps, *The Journal of Physical Chemistry C* **2018**, *122*, 22803-22820.
- [11] L. Silipigni, G. De Luca, T. Quattrone, L. M. Scolaro, G. Salvato, V. Grasso, *Journal of Physics: Condensed Matter* **2006**, *18*, 5759.
- [12] S. Golczak, A. Kancierzewska, M. Fahlman, K. Langer, J. J. Langer, *Solid State Ionics* **2008**, *179*, 2234-2239.
- [13] aG. Bhargava, I. Gouzman, C. Chun, T. Ramanarayanan, S. Bernasek, *Applied Surface Science* **2007**, *253*, 4322-4329; bD. Wang, J. Pan, H. Li, J. Liu, Y. Wang, L. Kang, J. Yao, *Journal of Materials Chemistry A* **2016**, *4*, 290-296.
- [14] L. Elbaz, G. Wu, P. Zelenay, in *Electrocatalysis in Fuel Cells*, Springer, **2013**, pp. 213-246.
- [15] D. Pantea, H. Darmstadt, S. Kaliaguine, L. Sümichen, C. Roy, *Carbon* **2001**, *39*, 1147-1158.
- [16] K. Artyushkova, I. Matanovic, B. Halevi, P. Atanassov, *The Journal of Physical Chemistry C* **2017**, *121*, 2836-2843.
- [17] Q. Dong, X. Zhuang, Z. Li, B. Li, B. Fang, C. Yang, H. Xie, F. Zhang, X. Feng, *Journal of Materials Chemistry A* **2015**, *3*, 7767-7772.

- [18] D. Malko, A. Kucernak, T. Lopes, *Nature Communications* **2016**, *7*, 13285.
- [19] N. D. Leonard, S. Wagner, F. Luo, J. Steinberg, W. Ju, N. Weidler, H. Wang, U. I. Kramm, P. Strasser, *ACS Catalysis* **2018**, *8*, 1640-1647.
- [20] aH. A. Gasteiger, N. M. Marković, *Science* **2009**, *324*, 48-49; bA. Friedman, L. Landau, S. Gonen, Z. Gross, L. Elbaz, *ACS Catalysis* **2018**, *8*, 5024-5031.
- [21] A. Friedman, I. Saltsman, Z. Gross, L. Elbaz, *Electrochimica Acta* **2019**.
- [22] N. R. Sahraie, U. I. Kramm, J. Steinberg, Y. Zhang, A. Thomas, T. Reier, J.-P. Paraknowitsch, P. Strasser, *Nature communications* **2015**, *6*, 8618.
- [23] aF. J. Uribe-Romo, J. R. Hunt, H. Furukawa, C. Klöck, M. O’Keeffe, O. M. Yaghi, *Journal of the American Chemical Society* **2009**, *131*, 4570-4571; bS. Kandambeth, V. Venkatesh, D. B. Shinde, S. Kumari, A. Halder, S. Verma, R. Banerjee, *Nature communications* **2015**, *6*, 6786; cP. Taynton, K. Yu, R. K. Shoemaker, Y. Jin, H. J. Qi, W. Zhang, *Advanced materials* **2014**, *26*, 3938-3942; dY.-h. Wu, L. Chen, J. Yu, S.-l. Tong, Y. Yan, *Dyes and Pigments* **2013**, *97*, 423-428.
- [24] S. Gonen, O. Lori, G. Cohen-Taguri, L. Elbaz, *Nanoscale* **2018**.
- [25] R. W. Pekala, *Journal of Materials Science* **1989**, *24*, 3221-3227.